

Neural Novel Actor: Learning a Generalized Animatable Neural Representation for Human Actors

Yiming Wang^{1*}, Qingzhe Gao^{2,1*}, Libin Liu^{1†}, Lingjie Liu^{3†}, Christian Theobalt³,
Baoquan Chen^{1†}

¹ Peking University, ² Shandong University, ³ Max Planck Institute for Informatics
{wym12416, libin.liu, baoquan}@pku.edu.cn, {lliu, theobalt}@mpi-inf.mpg.de gaoqingzhe97@gmail.com

Abstract

We propose a new method for learning a generalized animatable neural human representation from a sparse set of multi-view imagery of multiple persons. The learned representation can be used to synthesize novel view images of an arbitrary person from a sparse set of cameras, and further animate them with the user’s pose control. While existing methods can either generalize to new persons or synthesize animations with user control, none of them can achieve both at the same time. We attribute this accomplishment to the employment of a 3D proxy for a shared multi-person human model, and further the warping of the spaces of different poses to a shared canonical pose space, in which we learn a neural field and predict the person- and pose-dependent deformations, as well as appearance with the features extracted from input images. To cope with the complexity of the large variations in body shapes, poses, and clothing deformations, we design our neural human model with disentangled geometry and appearance. Furthermore, we utilize the image features both at the spatial point and on the surface points of the 3D proxy for predicting person- and pose-dependent properties. Experiments show that our method significantly outperforms the state-of-the-arts on both tasks. The video and code are available at https://talegqz.github.io/neural_novel_actor

1 Introduction

Synthesizing high-quality free-viewpoint videos of an arbitrary human character using a sparse set of cameras is crucial for many computer graphics applications, including VR/AR, film production, video games, and telepresence. Many of these applications require user control over human poses in the synthesis. Achieving these with traditional methods is difficult because it needs an expensive capturing setup (Debevec et al. 2000; Guo et al. 2019; Carranza et al. 2003; De Aguiar et al. 2008; Gall et al. 2009; Stoll et al. 2010), the production-quality human geometry and appearance models, and manual invention and corrections (Collet et al. 2015; Dou et al. 2016; Su et al. 2020).

Recently, neural human representation and rendering algorithms based on the neural radiance fields (NeRF) (Mildenhall et al. 2020) have demonstrated the ability to overcome the limitations of the traditional approaches. Some methods

(Liu et al. 2021a; Chen et al. 2021b; Peng et al. 2021a; Su et al. 2021) can learn an animatable human representation from multi-view imagery in a person-specific setting, but they are not able to generalize to new persons. Other works (Kwon et al. 2021; Zhao et al. 2021) proposed generalizable radiance fields for humans conditioned on input image features, inspired by the generalized neural representation for static scenes (Yu et al. 2021; Wang et al. 2021b; Chen et al. 2021a,a; Chibane et al. 2021; Liu et al. 2021b). With the learned representations, they can generate novel views of an arbitrary person from sparse multi-view images without training. However, their representations are not animatable and thus cannot generate images with user’s pose control.

In this paper, we present a new approach for learning a generalized animatable neural human representation from sparse multi-view input imagery of multiple persons. This representation allows us to generalize to new persons without training and further animate the representation with pose control. Specifically, our method uses a Skinned Multi-Person Linear (SMPL) model as a 3D proxy and transforms each pose space to a shared canonical pose space. Then a neural radiance field in the canonical space is learned and we estimate person- and pose-dependent geometry and appearance with the features extracted from the input images. To efficiently learn this representation for multiple persons, we disentangle the geometry and appearance in our human model by extracting separate features for geometry and appearance properties to condition the prediction of these properties. Furthermore, we extract the image features at both the spatial points and the surface points of SMPL to better infer the person- and pose-dependent properties.

We evaluate our method on the ZJU-MoCap (Peng et al. 2021b), DeepCap (Habermann et al. 2020) and DynaCap (Habermann et al. 2021) datasets. Compared with previous methods, our method achieves the generalization to new persons and the animation synthesis with user’s pose control. The experiments show that our method significantly outperforms the state-of-the-arts on both these tasks. In summary, our technical contributions are:

- We present a new method for achieving both the novel view synthesis of arbitrary persons and the animation synthesis with pose control at the same time.
- We design a new generalized animatable neural human representation with disentangled geometry and appear-

*These authors contributed equally.

†Corresponding authors

ance, which can be learned efficiently from sparse multi-view imagery of multiple persons.

- We present a new way to predict the person- and pose-dependent properties by taking the features at both the spatial points and the surface points of SMPL into account.

2 Related Work

2.1 Human Performance Capture

There have been multiple studies addressing novel view synthesis of human performance. Based on pre-scanned human models, many methods (Carranza et al. 2003; De Aguiar et al. 2008; Gall et al. 2009; Stoll et al. 2010) can capture humans in a sparse multi-view setting, but the pre-scanned human models are not available in most cases. Some recent work only relies on depth sensors (Collet et al. 2015; Dou et al. 2016; Su et al. 2020) or dense array of cameras (Debevec et al. 2000; Guo et al. 2019) to achieve high fidelity reconstruction, but these settings are not easily accessible. With the use of neural networks, methods (Martin-Brualla et al. 2018; Wu et al. 2020; Meshry et al. 2019) can compensate for geometric artifacts by modifying the rendering pipeline. More recently, some works (Saito et al. 2019; Natsume et al. 2019; Rahaman et al. 2019; Zheng et al. 2019; Saito et al. 2020; Huang et al. 2020; He et al. 2021) can reconstruct 3D humans from a single image with 3D human geometry priors. However, they rely on 3D geometry data and cannot generalize to complex poses not in training data. Unlike existing works, Our method can generalize to new persons just with sparse multi-view images supervision.

2.2 Neural Representations for human

With neural rendering (Shysheya et al. 2019; Thies, Zollhöfer, and Nießner 2019; Liu et al. 2020; Wu et al. 2020; Kwon et al. 2020a), neural networks can learn the reconstruction for 3d objects from 2D images. Many 3D representations, such as 3D voxel-grid (Lombardi et al. 2019; Sitzmann et al. 2019; Kwon et al. 2020b; Yan et al. 2016), point clouds (Aliev et al. 2020; Wu et al. 2020), textured mesh (Liu et al. 2019; Liao et al. 2020; Xiang et al. 2021; Thies, Zollhöfer, and Nießner 2019), and multi-plane images (Flynn et al. 2019; Zhou et al. 2018; Tucker and Snavely 2020), are learned from 2D images via differential rendering to improve the performance of novel view synthesis. However, it is difficult to get higher resolution due to memory restrictions. NeRF (Mildenhall et al. 2020) represents scenes with implicit fields of density and color. To extract more accurate surfaces, some works (Yariv et al. 2020; Niemeyer et al. 2020; Yariv et al. 2021; Wang et al. 2021a) learn the SDF to represent geometry in a scene. Based on these representations, many works (Gao et al. 2020; Peng et al. 2021b; Pumarola et al. 2021; Chen et al. 2021c; Xian et al. 2021; Noguchi et al. 2021; Su et al. 2021; Weng et al. 2022; Xu, Fujita, and Matsumoto 2022) employ neural representation to capture humans, but it is time-consuming to optimize for each novel video. Generalizable neural representation methods (Yu et al. 2021; Wang et al. 2021b; Chen et al. 2021a; Chibane et al. 2021; Liu et al. 2021b) avoid this

problem by using implicit fields conditioned on image features. Inspired by these work, some works (Kwon et al. 2021; Zhao et al. 2021) proposed generalizable radiance fields for humans, but they cannot obtain an animatable human model. Based on skinned multi-person linear model (SMPL) (Loper et al. 2015), some works (Liu et al. 2021a; Chen et al. 2021b; Peng et al. 2021a; Su et al. 2021; anonymous 2022) can get an animatable neural representation for humans. However, they still need subject-specific training. In contrast, we propose a novel deformable neural human representation, which enables us to obtain an animatable neural human representation from a single multi-view image of a new person without training. The concurrent work, MPS-NeRF (Gao et al. 2022), can also learn an animatable neural human representation from multi-view images of a single frame of the target person. It mainly relies on inverse skinning weights of SMPL (Loper et al. 2015) to animate the representation, while our method learns an additional residual deformation mapping to compensate for the deformation that cannot be modeled by inverse kinematic transformation. Furthermore, the representation of MPS-NeRF is based on NeRF (Mildenhall et al. 2020), while our representation additionally disentangles geometry and appearance by formulating them as two separate template implicit functions based on NeuS (Wang et al. 2021a).

3 Method

Given a set of multi-view RGB videos of several persons performing various motions, our goal is to learn a generalized animatable neural human representation (Fig. 1) in the training. At inference time, our model enables two tasks: (1) Generalization: given a sparse multi-view (e.g., 3 or 4 views) videos of an unseen person performing arbitrary motions, we can synthesize novel views of the person performing these motions without training. (2) Animation: given a sparse multi-view images of an unseen person in a static pose, we can animate the neural representation of the person to generate novel pose images according to the user’s pose control.

Our method uses the Skinned Multi-Person Linear (SMPL) model (Loper et al. 2015) as a 3D proxy and learns a canonical pose space shared by all the persons and poses. For each 3D point in a posed space, we convert it into this canonical space using the inverse skinning transformations (Huang et al. 2020) and the non-rigid deformations predicted by a neural network. Then, we learn a neural field (Wang et al. 2021a) in the canonical space to infer Signed Distance Fields (SDF) and color for generating the final images. Our key idea is to extract geometry and appearance features for each 3D point from the sparse input images and use these features to infer the non-rigid residual deformations, SDF and color at the 3D point. To better train our model on multiple persons, we propose two new designs: (1) We disentangle geometry and appearance by formulating them as two separate template implicit functions in the canonical space. (2) We extract the geometry and appearance features at both the 3D point and its nearest SMPL vertices; the rationale is that our model is a person-agnostic model and the 3D proxy (i.e., SMPL model) for different persons is shared. Therefore, taking the properties at both the 3D point and its SMPL surface points into consideration would better infer the distance of the 3D

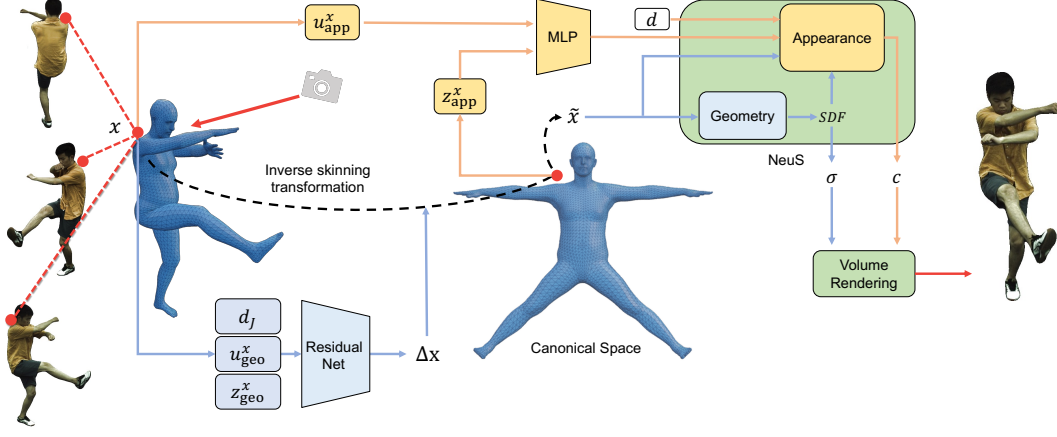


Figure 1: Overview of our framework. Given a query point x in the posed space, we use inverse skinning transformation of its nearest surface point and a predicted residual deformation to transform x to the canonical space. The deformed point \tilde{x} is used as input to our geometry network and appearance network. The pose-dependent residual deformation is predicted using geometry features $u_{\text{geo}}^x, z_{\text{geo}}^x$ and the relative displacement d_j between the query point x and every joint. The appearance features $u_{\text{app}}^x, z_{\text{app}}^x$ are used as input to the appearance network. The appearance network also takes the view direction d as input.

point to the SMPL surface for different persons.

In the following, we first introduce our deformable neural human representation (Sec. 3.1) and then explain how we construct the geometry and appearance features used in such a representation (Sec. 3.2). Based on our neural representation, we can synthesize novel view images for arbitrary human poses (Sec. 3.3).

3.1 Deformable Neural Human Representation

In order to represent different human identities and poses, we adopt SMPL (Loper et al. 2015) as the base model in our framework. SMPL is a mesh-based human model consisting of a template mesh with $N_v = 6890$ vertices $V \in \mathbb{R}^{N_v \times 3}$ and driven by N_J joints. It deforms the template mesh according to a set of parameters, ρ , representing the body shape and pose of a person. This process can be written as

$$v_\rho = \text{SMPL}(v, \rho, w_v), \quad (1)$$

where $v \in V$ represents a surface vertex and w_v is the skinning weight of v . We consider a predefined pose ρ_0 as the canonical model of our framework. The canonical space is then defined as the corresponding 3D space containing this canonical model. For an arbitrary pose ρ , we can transform the spacial points in the corresponding posed space into this canonical space using the SMPL surface as guidance. Such transformation links the canonical space to different posed spaces and thus allow those spaces to share the common features defined in the canonical space.

3.2 Geometry and appearance features

Our framework utilizes two latent variables, F_{geo} and F_{app} , to represent the geometry and appearance features of a person, respectively. These features are extracted from the input images and then used to render new images of the person performing novel poses from novel views. Our framework

obtains the geometry and appearance features in a similar manner, so we omit the subscripts in this section for simplicity when it is not confusing.

Both the geometry and appearance features are defined at every spacial point around the human model. The latent variable F defined at a spacial point x consists of two components $F = (u^x, z^x)$, where u^x represents the image features based on pixel alignment, and z^x are surface features computed based on the connectivity of the SMPL mesh.

Occlusion-aware image features Formally, our framework takes a sparse set of multi-view images, $\{I^c\}, c = 1, \dots, N_C$, captured by N_C calibrated cameras as input, where each image $I^c \in \mathbb{R}^{H \times W \times (3+1)}$ contains the RGB color of every pixel and a foreground mask indicating the pixels belong to the person. We apply CNN (Krizhevsky, Sutskever, and Hinton 2012) to these images and extract a set of feature maps U^c at multiple resolutions as

$$U^c = \text{CNN}([I^c]). \quad (2)$$

Then, for every spacial point x , we obtain a set of image features $\{u^c\}$ by projecting x onto each feature map U^c . Inspired by (Kwon et al. 2021), we employ a self-attention mechanism to aggregate these image features from different views to compute the image features u^x at x as

$$u^x = \text{softmax}_c \left(\frac{Q(u^c) \cdot K(u^c)}{\sqrt{d}} + B^c \right) \cdot V(u^c), \quad (3)$$

where $Q(\cdot)$, $K(\cdot)$, and $V(\cdot)$ are the learnable query, key, and value embedding functions proposed in the original self-attention mechanism (Vaswani et al. 2017), and d is the dimension of the embedding space.

When a spacial point is occluded in an input image I^c , its corresponding image features u^c is not reliable and should not be weighted the same as the features from the other images. We thus employ an occlusion-aware mechanism to

ensure this principle. Specifically, when a 3D query point \mathbf{x} is occluded by the posed SMPL model in an input image I^c , we subtract a fixed bias B^c from the corresponding attention weights in Equation (3) to explicitly inform the self-attention mechanism of this occlusion. This mechanism is partially inspired by Attention with Linear Biases (ALiBi) (Press, Smith, and Lewis 2021). We find that it effectively mitigates the artifacts caused by occlusion in our experiments.

Pose-aware surface features The mesh structure of the SMPL model provides a strong prior for determining the shape and appearance of human body. To fully utilize such structural cues, we associate surface features to the mesh and diffuse them to the spacial points in the surrounding space.

To build these surface features, we extract the occlusion-aware image features of every vertex of the mesh from the image and employ the Graph Convolution Networks (GCN) to fuse them as suggested by (Kipf and Welling 2016; Pfaff et al. 2020; Sanchez-Gonzalez et al. 2020). GCN is a special convolutional network structure that aggregates the information on each individual vertex based on the connectivity of the mesh. We additionally include the displacement between each pair of connected vertices in this operation. Considering that the SMPL mesh is deformed based on pose parameters, this augmentation effectively allows the GCN to encode an implicit pose description into the computation, thus resulting in a set of pose-aware features.

Formally, assuming the input images correspond to pose parameters ρ_I , we compute a deformed mesh V_{ρ_I} using SMPL and project each vertex $\mathbf{v} \in V_{\rho_I}$ onto the input images, obtaining a set of occlusion-aware image features $\{\mathbf{u}^v\}$. Then, we convert these image features using the pose-aware GCN described above and compute surface features

$$\{\mathbf{z}_I^v\} = \text{GCN}(\{\mathbf{u}^v\}, V_{\rho_I}). \quad (4)$$

When rendering a new pose ρ , we transform these input surface features $\{\mathbf{z}_I^v\}$ onto the corresponding new SMPL mesh V_ρ via another GCN procedure

$$\{\mathbf{z}^v\} = \text{GCN}(\{\mathbf{z}_I^v\}, V_\rho). \quad (5)$$

Note that these surface features, $\{\mathbf{z}^v\}$, are defined only on the surface vertices $\mathbf{v} \in V_\rho$. We then extend them to the surrounding space through a diffusion process. Specifically, for a spatial point \mathbf{x} in the vicinity of the deformed mesh V_ρ , we find K nearest vertices $\{\mathbf{v}^k\} \subset V_\rho$ on the mesh and take their features $\{\mathbf{z}^k\}$. The surface feature \mathbf{z}^x of the query point \mathbf{x} is then computed as

$$\mathbf{z}^x = \sum_k w_k \text{MLP}(\mathbf{z}^k, \mathbf{x} - \mathbf{v}^k), \quad (6)$$

where $w_k = (\|\mathbf{x} - \mathbf{v}^k\| + \epsilon)^{-1} / \sum_k (\|\mathbf{x} - \mathbf{v}^k\| + \epsilon)^{-1}$, and ϵ is a small scalar used to prevent dividing by zero.

Implementation For a spacial point \mathbf{x} , the latent variable $\mathbf{F}_{\text{geo}} = (\mathbf{u}_{\text{geo}}^x, \mathbf{z}_{\text{geo}}^x)$ and $\mathbf{F}_{\text{app}} = (\mathbf{u}_{\text{app}}^x, \mathbf{z}_{\text{app}}^x)$ are computed using the images features and the surface features defined above. To further enforce disentanglement of the features, we let the appearance features \mathbf{F}_{app} be independent of the driving pose ρ . This is achieved by computing $\mathbf{z}_{\text{app}}^x$ using the canonical pose ρ_0 in Equation (5), as depicts in Figure 1.

3.3 Pose-driven Volume Rendering

Using the geometry and appearance features \mathbf{F}_{geo} and \mathbf{F}_{app} extracted from the input images, our framework can render new images from a novel viewpoint given an arbitrary driving pose ρ . We employ NeuS (Wang et al. 2021a), an SDF-based differential renderer, to synthesize those images. NeuS predicts the color of each pixel by accumulating the radiance along the camera ray \mathbf{r} passing through the pixel. This computation can be discretized using a series of spacial points $\{\mathbf{x}_i\}$ sampled along \mathbf{r} . Specifically, NeuS computes

$$\tilde{C}(\mathbf{r}) = \sum_{i=1}^n T_i \alpha_i c_i, \quad (7)$$

where $\tilde{C}(\mathbf{r})$ is the predicted color, $T_i = \prod_{j=1}^{i-1} (1 - \alpha_j)$ is the discrete accumulated transmittance, α_i represents the opacity values defined as

$$\alpha_i = \max \left(\frac{\phi(s_i) - \phi(s_{i+1})}{\phi(s_i)}, 0 \right), \quad (8)$$

and $\phi(x) = (1 + e^{-kx})^{-1}$ with is a learnable scalar k . The color values c_i and the SDF values s_i in the above equations are evaluated at every sample point \mathbf{x}_i . Our framework handles every sample point in the same way, so we omit the subscript i in the rest of this section for simplicity.

Pose-driven deformation field Given a driving pose ρ , we transform each sample point \mathbf{x} into the canonical space and evaluate c and s based on the canonical position $\tilde{\mathbf{x}}$. This mechanism is inspired by recent studies (Tretschk et al. 2021; Liu et al. 2021a), which have shown its efficiency in modeling dynamic scenes and human poses. We define the deformation mapping Φ using the inverse skinning transformation (Huang et al. 2020). As suggested by (Liu et al. 2021a), an additional residual deformation mapping $\delta\Phi$ is employed to compensate for the deformation that cannot be captured by the inverse skinning, such as the deformation of cloth. The canonical position $\tilde{\mathbf{x}}$ of a sample point \mathbf{x} is thus computed as

$$\tilde{\mathbf{x}} = \Phi(\mathbf{x}, \rho) + \delta\Phi(\mathbf{x}, \rho). \quad (9)$$

$\Phi(\mathbf{x}, \rho)$ is the inverse skinning mapping

$$\Phi(\mathbf{x}, \rho) = \sum_{j=1}^{N_J} w_j \cdot (R_j(\mathbf{x} - \delta\mathbf{v}) + \mathbf{t}_j), \quad (10)$$

where R_j and \mathbf{t}_j represent the rotation and translation that transform joint j from pose ρ back to the canonical pose ρ_0 , $w_j \in \mathbf{w}_v$ is the corresponding skinning weight of the surface point \mathbf{v} that is the nearest to \mathbf{x} , and N_J is the number of joints. Note that we allow the pose parameters to also define the body shape of the target person. A displacement $\delta\mathbf{v}$ is leveraged to compensate for the deformation caused by the change of body shape. Specifically,

$$\delta\mathbf{v} = \text{SMPL}(\mathbf{v}, \beta(\rho), \mathbf{w}_v) - \text{SMPL}(\mathbf{v}, \beta(\rho_0), \mathbf{w}_v), \quad (11)$$

where $\beta(\cdot)$ extract the body shape parameters from ρ .

The residual deformation $\delta\Phi$ is computed using the geometry features $\mathbf{F}_{\text{geo}}^x$ extracted from the input images. We further consider the relative displacement between the query point \mathbf{x} and every joint, collectively represented by \mathbf{d}_J , as an extra cue. The residual displacement is thus computed as

$$\delta\Phi(\mathbf{x}, \rho) = \text{MLP}(\mathbf{F}_{\text{geo}}^x, \mathbf{d}_J). \quad (12)$$

SDF-based volume rendering After transforming the sample points \mathbf{x} into the canonical space $\tilde{\mathbf{x}}$ using the deformation field, we compute its SDF value s and color c as

$$s = \mathcal{S}(\tilde{\mathbf{x}}) \quad (13)$$

$$c = \mathcal{C}(\tilde{\mathbf{x}}, \mathbf{F}_{\text{app}}, \mathbf{d}, s, \mathbf{n}_x). \quad (14)$$

Both \mathcal{S} and \mathcal{C} are implemented as MLPs. The SDF function \mathcal{S} only takes the canonical position of \mathbf{x} as input. The color function \mathcal{C} considers the appearance feature \mathbf{F}_{app} , the view direction \mathbf{d} , the SDF value s of the sample point, as well as the normal vector \mathbf{n}_x of the implicit surface at the sample point. \mathbf{n}_x can be computed as the gradient of the SDF function $\mathbf{n}_x = \nabla_{\mathbf{x}} \mathcal{S}(\mathbf{x})$. The results of these functions are then used by NeuS to predict the color of the pixel as described above.

3.4 Training

For every training image, we render m random pixels and sample n spacial points on each generated camera ray. The loss function is then defined as

$$\begin{aligned} \mathcal{L} = & \frac{1}{m} \sum_r \underbrace{\|\tilde{C}(r) - C(r)\|_1}_{\text{color loss}} + \lambda_1 \sum_r \underbrace{\text{BCE}(\tilde{M}_r, M_r)}_{\text{mask loss}} \\ & + \lambda_2 \frac{1}{nm} \sum_{\mathbf{x}} \underbrace{(\|\mathbf{n}_{\mathbf{x}}\|_2 - 1)^2}_{\text{eikonal term}} + \lambda_3 \underbrace{\text{LPIPS}(\tilde{C}(P), C(P))}_{\text{LPIPS loss}}, \end{aligned} \quad (15)$$

where the color loss measures the difference between the predicted color $\tilde{C}(r)$ and the ground truth $C(r)$, the mask loss matches the predicted mask $\tilde{M}_r = \sum_{i=1}^n T_i \alpha_i$ with the foreground mask M_r by computing the binary cross entropy (BCE) between them, and an Eikonal term (Gropp et al. 2020) is adopted to regularize the SDF function. We further employ a perceptual loss, LPIPS (Zhang et al. 2018), to ensure the quality of the synthesized image. This LPIPS loss is computed by rendering random patches P sampled on the target image. We use the Adam optimizer (Kingma and Ba 2015) for training our model. More details of the training can be found in supplementary material.

4 Experiment

We conduct experiments on the ZJU-MoCap (Peng et al. 2021b), DeepCap (Habermann et al. 2020) and DynaCap (Habermann et al. 2021) datasets. We measure the quality with three evaluation metrics: Peak Signal-to-Noise Ratio (PSNR), Structural Similarity Index Measure (SSIM), and Learned Perceptual Image Patch Similarity (LPIPS) (Zhang et al. 2018). More details of the evaluations and datasets are provided in the supplementary material.

4.1 Generalization

In this part, we evaluate our approach on the generalization task. Given a sparse multi-view (e.g., 3 or 4 views) videos of an unseen person performing arbitrary motions, our method can synthesize novel views of the person performing these motions without training. Neural Human Performer (NHP) (Kwon et al. 2021) is the most related work to our method in

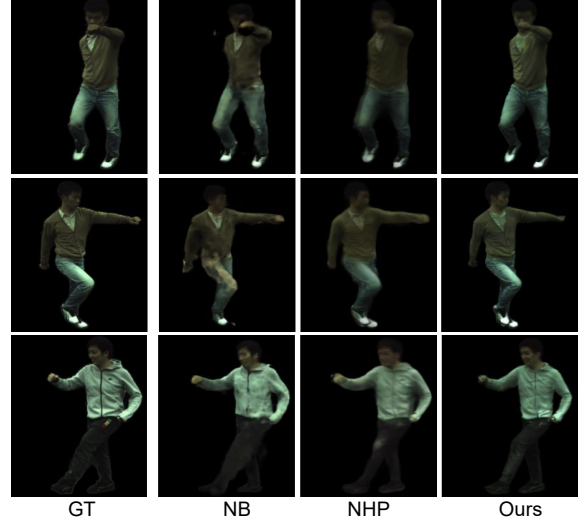


Figure 2: Qualitative comparison of identity generalization on the ZJU-MoCap dataset. Our method significantly outperforms two baselines, Neural Body (NB) (Peng et al. 2021b) and Neural Human Performer (NHP) (Kwon et al. 2021), in terms of synthesized wrinkles and appearance details. Note that NB is **overfitted to each target subject**, while NHP and our method are **trained on all the source subjects** and directly **tested on the target subjects** without training.

this setting, which also learns generalizable neural radiance fields based on SMPL. We also compare our method with Neural Body (NB) (Peng et al. 2021b) which is a person-specific model, so NB is trained in a per-subject manner in all the experiments. Note that we evaluated NHP and NB with their officially released checkpoints.

ZJU-MoCap dataset consists of 10 human subjects captured from 23 synchronized cameras. Following NHP, we split the dataset into two parts: 7 **source** subjects and 3 **target** subjects. We evaluate our method and the baseline methods in the following four different settings. Note that for all the comparisons except the cross-dataset generalization, the first 300 frames of the source or target subjects are used for training, and the rest frames (unseen poses) are used for testing.

1) Identity generalization. First, we evaluate the generalization to different identities by testing on the **target subjects**. Note that NB is trained on each target subject directly as it is a person-specific model, while NHP and our method are trained on all the source subjects and directly tested on target subjects. As Tab. 1 and Fig. 2 show, our method gives the best performances quantitatively and qualitatively. Our method even outperforms NB which is overfitted to the target subject.

2) Cross-dataset generalization. To further test the generalizability of our method to new datasets, we train our method and NHP on the ZJU-MoCap dataset and directly test on the DeepCap and DynaCap dataset without fine-tuning. As shown in the Tab. 1, our method significantly improves the performance compared to NHP. Even though the training and testing datasets are significantly different in the appearance distribution and the distance from the camera to subject,

Table 1: Quantitative comparison of the generalization task in the four settings. We evaluate the synthesis quality on three metrics: PSNR, SSIM and LPIPS. We compare with another generalized model, Neural Human Performer (NHP) (Kwon et al. 2021), and our method achieves significantly better performance in all the four settings. We also provide the results of a person-specific model, Neural Body (NB) (Peng et al. 2021b), as reference. Even though NB is directly trained on each target subject and tested on the same subject, our method is still better or on par with NB in all the four settings.

| Setting | Identity generalization | | | Cross-dataset | | | Pose generalization | | | Seen poses of seen subjects | | |
|---------|-------------------------|-----------------|--------------------|-----------------|-----------------|--------------------|---------------------|-----------------|--------------------|-----------------------------|-----------------|--------------------|
| Method | PSNR \uparrow | SSIM \uparrow | LPIPS \downarrow | PSNR \uparrow | SSIM \uparrow | LPIPS \downarrow | PSNR \uparrow | SSIM \uparrow | LPIPS \downarrow | PSNR \uparrow | SSIM \uparrow | LPIPS \downarrow |
| NB | 23.03 | 0.880 | 0.153 | - | - | - | 25.09 | 0.899 | 0.144 | 28.56 | 0.943 | 0.089 |
| NHP | 24.85 | 0.908 | 0.162 | 20.46 | 0.799 | 0.248 | 26.19 | 0.915 | 0.172 | 26.90 | 0.927 | 0.159 |
| Ours | 25.15 | 0.914 | 0.112 | 23.60 | 0.880 | 0.132 | 27.61 | 0.930 | 0.100 | 28.04 | 0.937 | 0.092 |

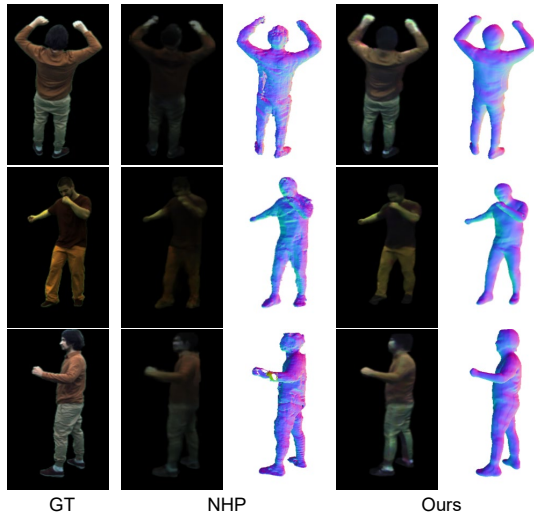


Figure 3: Qualitative comparison of cross-dataset generalization on novel view synthesis and 3D reconstruction. Neural Human Performer (NHP) (Kwon et al. 2021) and our method are trained on the ZJU-MoCap and directly tested on the DeepCap and DynaCap. Our method significantly outperforms NHP on novel view synthesis and geometry reconstruction.

our method still can achieve impressive results without fine-tuning, as shown in Fig. 3.

3) Pose generalization. In this setting, all the methods are trained on the source subjects and tested on **unseen poses of the same subject**. NHP and our method are trained on all source subjects together, while NB is trained per subject. As Tab. 1 shows, our model outperforms the baselines significantly on all the three metrics.

4) Seen poses of seen subjects. To demonstrate the superiority of our model, we evaluate the performance for seen poses of source subjects. NHP and our method are trained on the all source subjects and tested on the seen poses of them. Tab. 1 demonstrates that our method outperforms NHP, and it is comparable to NB, even though NB is trained directly on the target subject.

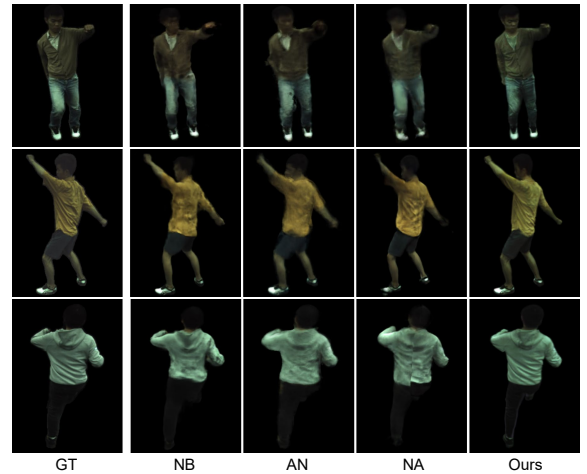


Figure 4: Qualitative comparison of the Animation task on the ZJU-MoCap dataset. We compared with three person-specific methods, Neural Body (NB)(Peng et al. 2021b), Animatable Nerf (AN) (Peng et al. 2021a) and Neural Actor (NA)(Liu et al. 2021a). Note that the baseline methods are trained with 300 frames of a target person and tested on the same person, while our method is trained on all source subjects and obtains an animatable human model of a target person just from **one** frame of the person. Our method outperforms all baselines even in a disadvantaged setting.

4.2 Animation

The task of animation is that, given a sparse multi-view images of an **unseen** person in a static pose, the model needs to generate novel pose images under user’s pose control. To evaluate the performance of this task, we compare our method with Neural Body (NB), Animatable Nerf (AN) (Peng et al. 2021a) and Neural Actor (NA) (Liu et al. 2021a) on the ZJU-MoCap dataset. NHP is not an animatable human model and thus cannot generate images with user’s pose control. Our method is a generalized animatable human model for this task, and other methods are person-specific animatable models, so they cannot directly apply to unseen subjects without training. Therefore, all the baselines are trained in a person-specific manner on the first 300 frames of the target person

Table 2: Quantitative comparison of the animation task. Our method achieves the best performance in all three metrics, compared to three person-specific animatable human models, NeuralBody (NB) (Peng et al. 2021b), AnimatableNerf (AN) (Peng et al. 2021a), and Neural Actor (NA) (Liu et al. 2021a). Note that our method is a generalized animatable human model, so our method is trained in a generalized setting which is more challenging than the person-specific setting of the baseline methods.

| Method | NB | AN | NA | Ours |
|--------------------|-------|-------|-------|--------------|
| PSNR \uparrow | 23.03 | 22.95 | 22.50 | 23.10 |
| SSIM \uparrow | 0.880 | 0.875 | 0.878 | 0.885 |
| LPIPS \downarrow | 0.153 | 0.197 | 0.173 | 0.145 |

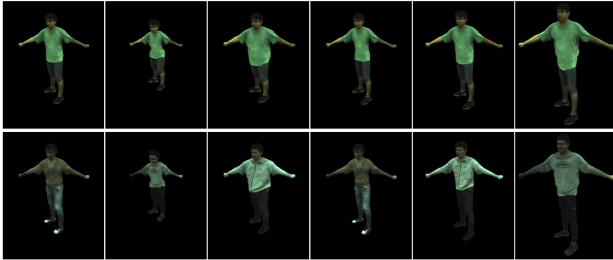


Figure 5: **Results of changing appearance and geometry.** We can directly change human shape (top row) and human appearance (bottom row) while keeping other factors fixed.

and tested on the remaining frames of the same person. In contrast, our model is trained on all the source subjects, and at test time, we directly obtain an animatable model of the target person just from the sparse camera views of one frame of the target person without training. The spilt for the ZJU-MoCap dataset is the same as that described in Sec. 4.1. Tab. 2 and Fig. 4 demonstrate that our method outperforms all baselines even though our method is trained and evaluated in a disadvantaged setting (i.e., unlike other baselines, our method is not overfitted to the target subject during training).

4.3 Appearance and geometry control

As our method disentangles the geometry and appearance in the human modeling, we can either change the appearance while keeping the geometry fixed or control the body shape of modeled humans by manipulating shape parameters in SMPL. Fig. 5 demonstrates the synthesized images after changing the body shape and exchanging the appearance.

4.4 Ablation Study

We conduct ablation studies using the ZJU-MoCap dataset on both the generalization and animation tasks. The same experiment settings as described in Sec. 4.1 and Sec. 4.2 are used for these two tasks. The results are shown in Table 3.

We first evaluate the effect of the GCN used in extracting the surface features. The baseline, w/o GCN, is performed by computing the surface features directly using the image features. It can be seen that removing the GCN operation leads to

Table 3: Ablation study for different components. Occ: the occlusion-aware self-attention mechanism, Sep: separation of geometry and appearance features.

| | Unseen subjects | | | Animation | | |
|----------------------|-----------------|-----------------|--------------------|-----------------|-----------------|--------------------|
| | PSNR \uparrow | SSIM \uparrow | LPIPS \downarrow | PSNR \uparrow | SSIM \uparrow | LPIPS \downarrow |
| w/o GCN | 24.27 | 0.891 | 0.121 | 22.81 | 0.872 | 0.146 |
| w/o u_{geo} | 23.79 | 0.890 | 0.133 | 22.34 | 0.875 | 0.154 |
| w/o u_{app} | 23.39 | 0.881 | 0.160 | 22.38 | 0.870 | 0.173 |
| w/o Occ | 24.10 | 0.889 | 0.140 | 22.79 | 0.874 | 0.158 |
| w/o Sep | 23.68 | 0.891 | 0.129 | 22.46 | 0.874 | 0.149 |
| w/o LPIPS | 25.30 | 0.912 | 0.150 | 23.50 | 0.890 | 0.176 |
| Full model | 25.15 | 0.914 | 0.112 | 23.10 | 0.885 | 0.145 |

a significant performance drop in both tasks, which indicates the efficiency of surface features discussed in Sec. 3.2.

We also evaluate the effect of the image features. We compare with: 1) removing the image features from the geometry features (w/o u_{geo}); 2) removing the image features from the appearance features (w/o u_{app}); 3) disabling the occlusion-aware self-attention mechanism (w/o Occ) by letting $B^c = 0$ in Equation (3). These comparisons show that the image features are critical to quality results, while our occlusion-aware mechanism effectively improves the perceptual realism.

To validate our design of disentangling the geometry and appearance features, we train a model with a single variable for both the appearance and geometry features (w/o Sep). As shown in Tab. 3, our disentangled features achieve better image quality in terms of all of the three metrics.

We further evaluate the effect of the LPIPS loss (w/o LPIPS) used in Equation (15). Note that it can be difficult for the metrics PSNR and SSIM to account for the nuances of human visual perception like LPIPS. Even though the images generated by the full model may have higher PSNR and SSIM than the baseline, they are usually clearer and thus more perceptually acceptable.

5 Conclusion

We presented Neural Novel Actor, a new method for learning a generalized animatable neural human representation from a sparse set of multi-view imagery of multiple persons. With the learned representation, we can synthesize novel view images of an arbitrary person using a sparse set of cameras and further synthesize animations with user’s pose control. To efficiently learn this representation for multiple persons, we design our proposed human representation with disentangled geometry and appearance. Furthermore, we leverage the features at both the spatial points and the surface points of SMPL to infer pose- and person-dependent geometry and appearance. Extensive experiments demonstrate that our method significantly outperforms the state-of-the-arts on the tasks of novel view synthesis of new persons and the animation synthesis with pose control.

Despite its success, our framework still has several limitations. First, our method relies on the accuracy of pose tracking, and the low-quality SMPL estimation may result in

artifacts. It would be interesting to optimize the SMPL parameters in the framework. Second, our method can only handle the clothing types that follow the topology of the SMPL model, and it is challenging to model very loose clothes, such as skirts. Finally, our method does not model complex lighting effects and we assume the uniform lighting in the input multi-view videos. When the assumption cannot be met (e.g., the ZJU-MoCap dataset), our model tends to learn the average lighting and produce the results with color shift.

Acknowledgments

This work was supported in part by NSFC Projects of International Cooperation and Exchanges (62161146002). Christian Theobalt was supported by ERC Consolidator Grant 4DReply (770784). Lingjie Liu was supported by Lise Meitner Postdoctoral Fellowship.

References

- Aliiev, K.-A.; Sevastopolsky, A.; Kolos, M.; Ulyanov, D.; and Lempitsky, V. 2020. Neural point-based graphics. In *European Conference on Computer Vision*, 696–712. Springer.
- anonymous. 2022. HDHumans: A Hybrid Approach for High-fidelity Digital Humans.
- Carranza, J.; Theobalt, C.; Magnor, M. A.; and Seidel, H.-P. 2003. Free-viewpoint video of human actors. *ACM transactions on graphics (TOG)*, 22(3): 569–577.
- Chen, A.; Xu, Z.; Zhao, F.; Zhang, X.; Xiang, F.; Yu, J.; and Su, H. 2021a. Mvsnrf: Fast generalizable radiance field reconstruction from multi-view stereo. In *Proceedings of the IEEE/CVF International Conference on Computer Vision*, 14124–14133.
- Chen, J.; Zhang, Y.; Kang, D.; Zhe, X.; Bao, L.; Jia, X.; and Lu, H. 2021b. Animatable neural radiance fields from monocular rgb videos. *arXiv preprint arXiv:2106.13629*.
- Chen, X.; Li, W.; Cohen-Or, D.; Mitra, N. J.; and Chen, B. 2021c. MoCo-Flow: Neural Motion Consensus Flow for Dynamic Humans in Stationary Monocular Cameras. *arXiv preprint arXiv:2106.04477*.
- Chibane, J.; Bansal, A.; Lazova, V.; and Pons-Moll, G. 2021. Stereo radiance fields (srf): Learning view synthesis for sparse views of novel scenes. In *Proceedings of the IEEE/CVF Conference on Computer Vision and Pattern Recognition*, 7911–7920.
- Collet, A.; Chuang, M.; Sweeney, P.; Gillett, D.; Evseev, D.; Calabrese, D.; Hoppe, H.; Kirk, A.; and Sullivan, S. 2015. High-quality streamable free-viewpoint video. *ACM Transactions on Graphics (ToG)*, 34(4): 1–13.
- De Aguiar, E.; Stoll, C.; Theobalt, C.; Ahmed, N.; Seidel, H.-P.; and Thrun, S. 2008. Performance capture from sparse multi-view video. In *ACM SIGGRAPH 2008 papers*, 1–10. ACM New York, NY, USA.
- Debevec, P.; Hawkins, T.; Tchou, C.; Duiker, H.-P.; Sarokin, W.; and Sagar, M. 2000. Acquiring the reflectance field of a human face. In *Proceedings of the 27th annual conference on Computer graphics and interactive techniques*, 145–156.
- Dou, M.; Khamis, S.; Degtyarev, Y.; Davidson, P.; Fanello, S. R.; Kowdle, A.; Escolano, S. O.; Rhemann, C.; Kim, D.; Taylor, J.; et al. 2016. Fusion4d: Real-time performance capture of challenging scenes. *ACM Transactions on Graphics (ToG)*, 35(4): 1–13.
- Flynn, J.; Broxton, M.; Debevec, P.; DuVall, M.; Fyffe, G.; Overbeck, R.; Snavely, N.; and Tucker, R. 2019. Deepview: View synthesis with learned gradient descent. In *Proceedings of the IEEE/CVF Conference on Computer Vision and Pattern Recognition*, 2367–2376.
- Gall, J.; Stoll, C.; De Aguiar, E.; Theobalt, C.; Rosenhahn, B.; and Seidel, H.-P. 2009. Motion capture using joint skeleton tracking and surface estimation. In *2009 IEEE Conference on Computer Vision and Pattern Recognition*, 1746–1753. IEEE.
- Gao, C.; Shih, Y.; Lai, W.-S.; Liang, C.-K.; and Huang, J.-B. 2020. Portrait neural radiance fields from a single image. *arXiv preprint arXiv:2012.05903*.
- Gao, X.; Yang, J.; Kim, J.; Peng, S.; Liu, Z.; and Tong, X. 2022. MPS-NeRF: Generalizable 3D Human Rendering from Multiview Images. *arXiv preprint arXiv:2203.16875*.
- Gropp, A.; Yariv, L.; Haim, N.; Atzmon, M.; and Lipman, Y. 2020. Implicit geometric regularization for learning shapes. *arXiv preprint arXiv:2002.10099*.
- Guo, K.; Lincoln, P.; Davidson, P.; Busch, J.; Yu, X.; Whalen, M.; Harvey, G.; Orts-Escolano, S.; Pandey, R.; Dourgarian, J.; et al. 2019. The relightables: Volumetric performance capture of humans with realistic relighting. *ACM Transactions on Graphics (ToG)*, 38(6): 1–19.
- Habermann, M.; Liu, L.; Xu, W.; Zollhoefer, M.; Pons-Moll, G.; and Theobalt, C. 2021. Real-time deep dynamic characters. *ACM Transactions on Graphics (TOG)*, 40(4): 1–16.
- Habermann, M.; Xu, W.; Zollhofer, M.; Pons-Moll, G.; and Theobalt, C. 2020. Deepcap: Monocular human performance capture using weak supervision. In *Proceedings of the IEEE/CVF Conference on Computer Vision and Pattern Recognition*, 5052–5063.
- He, T.; Xu, Y.; Saito, S.; Soatto, S.; and Tung, T. 2021. ARCH++: Animation-ready clothed human reconstruction revisited. In *Proceedings of the IEEE/CVF International Conference on Computer Vision*, 11046–11056.
- Huang, Z.; Xu, Y.; Lassner, C.; Li, H.; and Tung, T. 2020. Arch: Animatable reconstruction of clothed humans. In *Proceedings of the IEEE/CVF Conference on Computer Vision and Pattern Recognition*, 3093–3102.
- Kingma, D. P.; and Ba, J. 2015. Adam: A Method for Stochastic Optimization. In Bengio, Y.; and LeCun, Y., eds., *3rd International Conference on Learning Representations, ICLR 2015, San Diego, CA, USA, May 7-9, 2015, Conference Track Proceedings*.
- Kipf, T. N.; and Welling, M. 2016. Semi-Supervised Classification with Graph Convolutional Networks. *CoRR*, abs/1609.02907.
- Krizhevsky, A.; Sutskever, I.; and Hinton, G. E. 2012. Imagenet classification with deep convolutional neural networks. *Advances in neural information processing systems*, 25.

- Kwon, Y.; Kim, D.; Ceylan, D.; and Fuchs, H. 2021. Neural human performer: Learning generalizable radiance fields for human performance rendering. *Advances in Neural Information Processing Systems*, 34.
- Kwon, Y.; Petrangeli, S.; Kim, D.; Wang, H.; Park, E.; Swaminathan, V.; and Fuchs, H. 2020a. Rotationally-temporally consistent novel view synthesis of human performance video. In *European Conference on Computer Vision*, 387–402. Springer.
- Kwon, Y.; Petrangeli, S.; Kim, D.; Wang, H.; Park, E.; Swaminathan, V.; and Fuchs, H. 2020b. Rotationally-temporally consistent novel view synthesis of human performance video. In *European Conference on Computer Vision*, 387–402. Springer.
- Liao, Y.; Schwarz, K.; Mescheder, L.; and Geiger, A. 2020. Towards unsupervised learning of generative models for 3d controllable image synthesis. In *Proceedings of the IEEE/CVF Conference on Computer Vision and Pattern Recognition*, 5871–5880.
- Liu, L.; Habermann, M.; Rudnev, V.; Sarkar, K.; Gu, J.; and Theobalt, C. 2021a. Neural actor: Neural free-view synthesis of human actors with pose control. *ACM Transactions on Graphics (TOG)*, 40(6): 1–16.
- Liu, L.; Xu, W.; Habermann, M.; Zollhöfer, M.; Bernard, F.; Kim, H.; Wang, W.; and Theobalt, C. 2020. Neural human video rendering by learning dynamic textures and rendering-to-video translation. *arXiv preprint arXiv:2001.04947*.
- Liu, L.; Xu, W.; Zollhoefer, M.; Kim, H.; Bernard, F.; Habermann, M.; Wang, W.; and Theobalt, C. 2019. Neural rendering and reenactment of human actor videos. *ACM Transactions on Graphics (TOG)*, 38(5): 1–14.
- Liu, Y.; Peng, S.; Liu, L.; Wang, Q.; Wang, P.; Theobalt, C.; Zhou, X.; and Wang, W. 2021b. Neural Rays for Occlusion-aware Image-based Rendering. *arXiv preprint arXiv:2107.13421*.
- Lombardi, S.; Simon, T.; Saragih, J.; Schwartz, G.; Lehrmann, A.; and Sheikh, Y. 2019. Neural Volumes: Learning Dynamic Renderable Volumes from Images. *ACM Trans. Graph.*, 38(4): 65:1–65:14.
- Loper, M.; Mahmood, N.; Romero, J.; Pons-Moll, G.; and Black, M. J. 2015. SMPL: A skinned multi-person linear model. *ACM transactions on graphics (TOG)*, 34(6): 1–16.
- Martin-Brualla, R.; Pandey, R.; Yang, S.; Pidlypenskyi, P.; Taylor, J.; Valentin, J.; Khamis, S.; Davidson, P.; Tkach, A.; Lincoln, P.; et al. 2018. Lookingood: Enhancing performance capture with real-time neural re-rendering. *arXiv preprint arXiv:1811.05029*.
- Meshry, M.; Goldman, D. B.; Khamis, S.; Hoppe, H.; Pandey, R.; Snavely, N.; and Martin-Brualla, R. 2019. Neural rerendering in the wild. In *Proceedings of the IEEE/CVF Conference on Computer Vision and Pattern Recognition*, 6878–6887.
- Mildenhall, B.; Srinivasan, P. P.; Tancik, M.; Barron, J. T.; Ramamoorthi, R.; and Ng, R. 2020. Nerf: Representing scenes as neural radiance fields for view synthesis. In *European conference on computer vision*, 405–421. Springer.
- Natsume, R.; Saito, S.; Huang, Z.; Chen, W.; Ma, C.; Li, H.; and Morishima, S. 2019. Siclope: Silhouette-based clothed people. In *Proceedings of the IEEE/CVF Conference on Computer Vision and Pattern Recognition*, 4480–4490.
- Niemeyer, M.; Mescheder, L.; Oechsle, M.; and Geiger, A. 2020. Differentiable Volumetric Rendering: Learning Implicit 3D Representations without 3D Supervision. In *Proc. IEEE Conf. on Computer Vision and Pattern Recognition (CVPR)*.
- Noguchi, A.; Sun, X.; Lin, S.; and Harada, T. 2021. Neural articulated radiance field. In *Proceedings of the IEEE/CVF International Conference on Computer Vision*, 5762–5772.
- Peng, S.; Dong, J.; Wang, Q.; Zhang, S.; Shuai, Q.; Zhou, X.; and Bao, H. 2021a. Animatable neural radiance fields for modeling dynamic human bodies. In *Proceedings of the IEEE/CVF International Conference on Computer Vision*, 14314–14323.
- Peng, S.; Zhang, Y.; Xu, Y.; Wang, Q.; Shuai, Q.; Bao, H.; and Zhou, X. 2021b. Neural body: Implicit neural representations with structured latent codes for novel view synthesis of dynamic humans. In *Proceedings of the IEEE/CVF Conference on Computer Vision and Pattern Recognition*, 9054–9063.
- Pfaff, T.; Fortunato, M.; Sanchez-Gonzalez, A.; and Battaglia, P. W. 2020. Learning mesh-based simulation with graph networks. *arXiv preprint arXiv:2010.03409*.
- Press, O.; Smith, N. A.; and Lewis, M. 2021. Train Short, Test Long: Attention with Linear Biases Enables Input Length Extrapolation. *ArXiv*, abs/2108.12409.
- Pumarola, A.; Corona, E.; Pons-Moll, G.; and Moreno-Noguer, F. 2021. D-nerf: Neural radiance fields for dynamic scenes. In *Proceedings of the IEEE/CVF Conference on Computer Vision and Pattern Recognition*, 10318–10327.
- Rahaman, N.; Baratin, A.; Arpit, D.; Draxler, F.; Lin, M.; Hamprecht, F.; Bengio, Y.; and Courville, A. 2019. On the spectral bias of neural networks. In *International Conference on Machine Learning*, 5301–5310. PMLR.
- Saito, S.; Huang, Z.; Natsume, R.; Morishima, S.; Kanazawa, A.; and Li, H. 2019. Pifu: Pixel-aligned implicit function for high-resolution clothed human digitization. In *Proceedings of the IEEE/CVF International Conference on Computer Vision*, 2304–2314.
- Saito, S.; Simon, T.; Saragih, J.; and Joo, H. 2020. Pifuhd: Multi-level pixel-aligned implicit function for high-resolution 3d human digitization. In *Proceedings of the IEEE/CVF Conference on Computer Vision and Pattern Recognition*, 84–93.
- Sanchez-Gonzalez, A.; Godwin, J.; Pfaff, T.; Ying, R.; Leskovec, J.; and Battaglia, P. 2020. Learning to simulate complex physics with graph networks. In *International Conference on Machine Learning*, 8459–8468. PMLR.
- Shysheya, A.; Zakharov, E.; Aliev, K.-A.; Bashirov, R.; Burkov, E.; Isakov, K.; Ivakhnenko, A.; Malkov, Y.; Pasechnik, I.; Ulyanov, D.; et al. 2019. Textured neural avatars. In *Proceedings of the IEEE/CVF Conference on Computer Vision and Pattern Recognition*, 2387–2397.

- Sitzmann, V.; Thies, J.; Heide, F.; Nießner, M.; Wetzstein, G.; and Zollhofer, M. 2019. Deepvoxels: Learning persistent 3d feature embeddings. In Proceedings of the IEEE/CVF Conference on Computer Vision and Pattern Recognition, 2437–2446.
- Stoll, C.; Gall, J.; De Aguiar, E.; Thrun, S.; and Theobalt, C. 2010. Video-based reconstruction of animatable human characters. ACM Transactions on Graphics (TOG), 29(6): 1–10.
- Su, S.-Y.; Yu, F.; Zollhöfer, M.; and Rhodin, H. 2021. A-nerf: Articulated neural radiance fields for learning human shape, appearance, and pose. Advances in Neural Information Processing Systems, 34.
- Su, Z.; Xu, L.; Zheng, Z.; Yu, T.; Liu, Y.; and Fang, L. 2020. Robustfusion: Human volumetric capture with data-driven visual cues using a rgbd camera. In European Conference on Computer Vision, 246–264. Springer.
- Thies, J.; Zollhöfer, M.; and Nießner, M. 2019. Deferred neural rendering: Image synthesis using neural textures. ACM Transactions on Graphics (TOG), 38(4): 1–12.
- Tretschk, E.; Tewari, A.; Golyanik, V.; Zollhöfer, M.; Lassner, C.; and Theobalt, C. 2021. Non-Rigid Neural Radiance Fields: Reconstruction and Novel View Synthesis of a Dynamic Scene From Monocular Video. In Proceedings of the IEEE/CVF International Conference on Computer Vision, 12959–12970.
- Tucker, R.; and Snavely, N. 2020. Single-view view synthesis with multiplane images. In Proceedings of the IEEE/CVF Conference on Computer Vision and Pattern Recognition, 551–560.
- Vaswani, A.; Shazeer, N.; Parmar, N.; Uszkoreit, J.; Jones, L.; Gomez, A. N.; Kaiser, Ł.; and Polosukhin, I. 2017. Attention is All you Need. In Guyon, I.; Luxburg, U. V.; Bengio, S.; Wallach, H.; Fergus, R.; Vishwanathan, S.; and Garnett, R., eds., Advances in Neural Information Processing Systems, volume 30.
- Wang, P.; Liu, L.; Liu, Y.; Theobalt, C.; Komura, T.; and Wang, W. 2021a. NeuS: Learning Neural Implicit Surfaces by Volume Rendering for Multi-view Reconstruction. Advances in Neural Information Processing Systems, 34.
- Wang, Q.; Wang, Z.; Genova, K.; Srinivasan, P. P.; Zhou, H.; Barron, J. T.; Martin-Brualla, R.; Snavely, N.; and Funkhouser, T. 2021b. Ibrnet: Learning multi-view image-based rendering. In Proceedings of the IEEE/CVF Conference on Computer Vision and Pattern Recognition, 4690–4699.
- Weng, C.-Y.; Curless, B.; Srinivasan, P. P.; Barron, J. T.; and Kemelmacher-Shlizerman, I. 2022. HumanNeRF: Free-viewpoint Rendering of Moving People from Monocular Video. arXiv preprint arXiv:2201.04127.
- Wu, M.; Wang, Y.; Hu, Q.; and Yu, J. 2020. Multi-view neural human rendering. In Proceedings of the IEEE/CVF Conference on Computer Vision and Pattern Recognition, 1682–1691.
- Xian, W.; Huang, J.-B.; Kopf, J.; and Kim, C. 2021. Space-time neural irradiance fields for free-viewpoint video. In Proceedings of the IEEE/CVF Conference on Computer Vision and Pattern Recognition, 9421–9431.
- Xiang, F.; Xu, Z.; Hasan, M.; Hold-Geoffroy, Y.; Sunkavalli, K.; and Su, H. 2021. Neutex: Neural texture mapping for volumetric neural rendering. In Proceedings of the IEEE/CVF Conference on Computer Vision and Pattern Recognition, 7119–7128.
- Xu, T.; Fujita, Y.; and Matsumoto, E. 2022. Surface-Aligned Neural Radiance Fields for Controllable 3D Human Synthesis. arXiv preprint arXiv:2201.01683.
- Yan, X.; Yang, J.; Yumer, E.; Guo, Y.; and Lee, H. 2016. Perspective transformer nets: Learning single-view 3d object reconstruction without 3d supervision. Advances in neural information processing systems, 29.
- Yariv, L.; Gu, J.; Kasten, Y.; and Lipman, Y. 2021. Volume rendering of neural implicit surfaces. In Thirty-Fifth Conference on Neural Information Processing Systems.
- Yariv, L.; Kasten, Y.; Moran, D.; Galun, M.; Atzmon, M.; Ronen, B.; and Lipman, Y. 2020. Multiview Neural Surface Reconstruction by Disentangling Geometry and Appearance. Advances in Neural Information Processing Systems, 33.
- Yu, A.; Ye, V.; Tancik, M.; and Kanazawa, A. 2021. pixelnerf: Neural radiance fields from one or few images. In Proceedings of the IEEE/CVF Conference on Computer Vision and Pattern Recognition, 4578–4587.
- Zhang, R.; Isola, P.; Efros, A. A.; Shechtman, E.; and Wang, O. 2018. The Unreasonable Effectiveness of Deep Features as a Perceptual Metric. In CVPR.
- Zhao, F.; Yang, W.; Zhang, J.; Lin, P.; Zhang, Y.; Yu, J.; and Xu, L. 2021. HumanNeRF: Generalizable Neural Human Radiance Field from Sparse Inputs. arXiv preprint arXiv:2112.02789.
- Zheng, Z.; Yu, T.; Wei, Y.; Dai, Q.; and Liu, Y. 2019. Deephuman: 3d human reconstruction from a single image. In Proceedings of the IEEE/CVF International Conference on Computer Vision, 7739–7749.
- Zhou, T.; Tucker, R.; Flynn, J.; Fyffe, G.; and Snavely, N. 2018. Stereo magnification: Learning view synthesis using multiplane images. arXiv preprint arXiv:1805.09817.